Reactive and Functional Polymers 143 (2019) 104345

Contents lists available at ScienceDirect

Reactive and Functional Polymers

journal homepage: www.elsevier.com/locate/react

Monolithic nanoporous polymers bearing POSS moiety as efficient flame retardant and thermal insulation materials

Fei Wang, Huijuan Wei, Chao Liu, Hanxue Sun, Zhaoqi Zhu, Weidong Liang, An Li*

College of Petrochemical Technology, Lanzhou University of Technology, Langongping Road 287, Lanzhou 730050, PR China

ARTICLE INFO

Keywords:
POSS
Monolithic nanoporous polymers
Flame retardant
Thermal insulation

ABSTRACT

The creation of porous materials with both good thermal insulation and flame retardancy is of great importance for construction of energy-saving coatings in many applications. Herein, we report the facile fabrication of octasilsesquioxane (POSS)-based monolithic nanoporous polymers (named as PDVB-POSS) by solvothermal method using octavinyl-POSS as monomer and divinylbenzene (DVB) as crosslinker followed by freeze drying. The as-prepared PDVB-POSS show abundant porosity with mesopore sizes ranging from 8 nm to 13 nm, which results in a high thermal insulation with a low thermal conductivity of 0.024 $W m^{-1} k^{-1}$ in air. The PDVB-POSS also possesses excellent flame retardancy with a peak heat released rate (pHRR) of as low as 144 $W g^{-1}$. Torch burn test implies that the PDVB-POSS shows self-extinguishing behaviors without generation of any melt dripping, further reflecting an excellent flame retardancy. Taking advantages of simple fabrication process, easily to be scaled-up, excellent thermal insulation and flame retardancy, such POSS-based monolithic porous polymers may have great potential as energy-saving coatings for real applications.

1. Introduction

With the huge energy consumed by the rapid development of modern industry, human society is facing an increasingly serious energy crisis. More ominously, the enormous use of fossil fuels on the other hand has resulted in a number of severe environmental issues, including emerging ecological concerns and global warming, etc. Therefore, the development of alternative energy sources or improvement of energy efficiency is of great importance for construction of sustainable overall energy ecosystem. Nowadays, enormous amounts of fossil fuels have been consumed for heating and air conditioning in residential and commercial buildings each year. For example, residential and commercial buildings consume 40% of the total energy in the United States [1], with 33% used for heating and 7% for cooling [2]. To reduce the energy waste and enhance the energy utilization efficiency which in turn decrease the fossil fuels consumption, the use of materials with good thermal insulation for exterior wall insulation has been proven to be one of the most efficent way to this end. So far, a wide variety of natural or synthetic polymers with porous feature as well as low thermal conductivity (κ, W/(m·K)), including chitosan [3,4], cellulose [5], polystyrene [6], urethane [7], polyethylene [8] and so on [9,10], have been used as thermal insulation coatings for modern energy-saving building construction. However, these mentioned polymers are organic in nature and therefore very flammable, which would pose the serious problem of fire risk. In this regard, the requirements for high-performance thermal insulation materials are still very high, not only good thermal insulation performance but also superior flame retardant performance.

Low thermal conductivity is a prerequisite for thermal insulation materials. In fact, to achieve a better thermal insulation property, the creation of a porous structure on these materials with low thermal conductivity has been proven to be a more effective strategy which could be reflected by the following two factors, i.e., the porous structure would impede the solid-state heat conduction along the skeleton of the substrate materials, while small pores would facilitate to confine air in a small space to prevent thermal convection. Along this line, several kinds of porous materials with superior thermal insulation property have been developed, including aerogels [11,12], porous synthetic polymers [13,14], and natural polymers [15], to name a few. On the other hand, to endow the additional flame retardant properties on these mentioned thermal insulation materials, surface modification by physical or chemical methods has been well investigated to this end. For example, layer-by layer assembly has been extensively adopted to physically create flame-retardant coatings on various porous substrate materials with thermal insulation property [16–18]. Surface modification of these substrate materials by grafting-on approach has also been

* Corresponding author.
E-mail address: lian2010@lut.cn (A. Li).

https://doi.org/10.1016/j.reactfunctpolym.2019.104345
Received 21 June 2019; Received in revised form 22 August 2019; Accepted 23 August 2019
Available online 25 August 2019
1381-5148/

employed to chemically bond the flame-retardant moieties onto the target substrate materials to produce the disired performance [19]. Though significant progress have been achieved in terms of improving both thermal insulation and flame retardant properties by using these methods, big obstacle still remains as these methods have their respective limitations such as multistep processes, time consuming or highly complicated techniques, which hinders their practical applications. Even more, in some cases, these "adding" approaches may result in the impairment in the intrinsic properties, e.g., mechanical properties or optical properties, of the thermal insulation substrates. Such phenomenon would become more worse especially in a high loading of flame retardant where much more dopants are required to achieve effective fire retardancy.

In our previous works, we have reported the synthesis of nanoporous flame retardants with good thermal insulation properties based on benzotriazole-based conjugated microporous polymers and fluorine-rich conjugated microporous polymer [20,21]. In these cases, the excellent porosity combined with the flame-retardant moieties which are chemically bonded on the framework of conjugated microporous polymers are responsible to their desired flame retardancy and thermal insulation. As well as we known, octavinyl-POSS has been widely used to prepare POSS-based porous polymers by many other different ways [22–26]. Herein, we porpose a new approach for facile fabrication of POSS-based monolithic nanoporous polymers by solvothermal method using octavinyl-POSS as monomer and divinylbenzene as crosslinker followed by freeze drying. Our primary design lies in the employment of rigid POSS and aromatic ring as building blocks to construct a inherentely nanoporous network architecture to improve the thermal insulation, while the introduction of the flame retardant moieties, i.e., POSS units, into the skeleton of as-synthesized PDVB-POSS framework itself would produce better flame retardancy performance. As anticipated, the resulting POSS-based monolithic nanoporous polymers show low thermal conductivity as well as excellent flame retardancy, makes them ideal candidate as efficient flame retardant and thermal insulation materials.

2. Experimental details

2.1. Materials

Vinymethyltrimethoxysilane (VTMO) and divinylbenzene (DVB) were obtained from macklin Biochemical Technology Co., Ltd., Shanghai, China. 2,2′-Azobis(2-methylpropionitrile) was offered by BASF Chemical industry Co., Ltd., Tianjin, China. Tetrahydrofuran was obtained from Baishi Chemical Co., Ltd., Tianjin, China. All chemicals used as received with a purity of 98% or greater. The chemical structures of the materials are shown in Fig. S1.

2.2. Preparation of octavinyl-POSS

The octavinyl-POSS was synthesis by hydrolysis condensation reaction of vinymethyltrimethoxysilane (VTMO) [27], as shown in Fig. S2. Acetone (675 mL) and VTMO (67 g) were placed in a 1 L flask, which was mixed evenly under magnetic stirring. A mixed solution of concentrated hydrochloric acid (112.6 mL) and distilled water (130 mL) was added dropwise to the reactants, followed by reflux at 40 °C for 48 h. Thereafter, the reaction mixture turned brown and a white solid deposited on the flask wall. The solvent mixture was poured into a flask for recycling, the white solid was separated and washed with ethanol for three times and then dried at 60 °C. The crude product was recrystallized to obtain the octavinyl-POSS in a mixed solvent of dichloromethane and acetone (volume ratio 1:3). The molecular structural formula and simulation structure of octavinyl-POSS are shown in Fig. S3.

2.3. Preparation of porous polymers

Octavinyl-POSS (1.27 g), divinylbenzene (DVB, 1.04 g) and 2,2′-Azobis(2-methylpropionitrile) (AIBN, 50 mg) were placed in an autoclave (100 mL hydrothermal high pressure reactor, Xi'an Dexiang experimental equipment), and then 20 mL tetrahydrofuran (THF) with 2 mL distilled water were added. After stirring for half an hour at room temperature, the magnet was taken out. The solution was treated at 65 °C for 72 h. The system was cooled to room temperature and the solvent was replaced with distilled water. The solid monolith was obtained after freeze-drying (named as PDVB-POSS). Poly (divinylbenzene) (PDVB) was prepared as a comparative sample by the same preparation method. Digital photographs of PDVB-POSS before drying are shown in Fig. S4.

2.4. Characterization

Fourier transform infrared (FTIR) spectra were recorded in the wavelength range of 4000–400 cm^{-1} using the KBr pellet technique on a Nexus 670 spectrum instrument. ^{13}C cross-polarization magic angle Spinning (CP/MAS) NMR spectra were carried out on a Bruker AVANCE III 400 MHz NMR spectrometer at a resonance frequency of 100.6 MHz and recorded using a MAS probe 4 mm in diameter and a spinning rate of 14 kHz. The powder X-ray diffraction (XRD) patterns were recorded on a D/Max-2400 X-ray diffractometer (Rigaku Miniflex, Japan) using Cu-Ka radiation, operated at 40 kV and 100 mA from 2° to 80°. (The foams were grinded into powder for XRD test) The morphologies of PDVB and PDVB-POSS were observed by scanning electron microscope (SEM, JSM-6701F, JEOL, Ltd.), and the samples were sprayed with a layer of Au film before measurement. Energy-dispersive X-ray spectroscopy (EDX) was performed to obtain the relative elemental compositions of the samples at the surface and inner using an EDX apparatus (INCA type, British Oxford Instrument Co.). The thermal stability was investigated by thermogravimeter analysis (TGA) from ambient temperature to 800 °C at a heating rate of 10 °C min^{-1} under nitrogen atmosphere. The Brunauer-Emmett-Teller (BET) surface areas and pore structures of the samples were measured by a micromeritics ASAP 2020 apparatus at 77.3 K, all samples were degassed at 120 °C overnight under vacuum before analysis. The thermal conductivity values of samples were measured by a multi-function rapid thermal conductivity tester (DRE-III, China) by transient plane source method. The infrared thermal image is obtained with an infrared camera (Thermal Imager TESTO 869, Testo SE & Co. KGaA, Germany). Torch burn tests were evaluated by exposure to direct flame from a butane torch at a 45° angle for 10 s. (inner flame of the torch is light blue and 4 cm in length.) Microcalorimetry (MCC) tests were conducted on a MCC-1 microscale combustion calorimeter (GOVMARK, USA, ASTM D7309), the samples were dried at 75 °C for 8 h in a blower box before the test and about 5 mg samples were heated at a heating rate of 1 °C s^{-1} from 75 °C to 750 °C.

3. Results and discussion

3.1. Characterization of chemical structure

In this work, we first prepared octavinyl-POSS by hydrolysis condensation reaction under acid catalysis. Subsequently, the porous polymer based on octavinyl-POSS (PDVB-POSS) are prepared by solvothermal method using octavinyl-POSS as monomer, AIBN as initiator, DVB as crosslinking agent in the miscible liquids of THF and distilled water, the specific synthesis route of PDVB-POSS is shown in Fig. 1. Two kinds of PDVB-POSS were prepared according to the molar ratio of the monomer (octavinyl-POSS) to crosslinker (DVB) of 1:4 (named as PDVB-POSS (1:4)) and 1:2 (named as PDVB-POSS (1:2)), respectively.

The molecular level structure of octavinyl-POSS, PDVB and PDVB-POSS were confirmed by NMR, as shown in Fig. 2. As shown in Fig. 2a

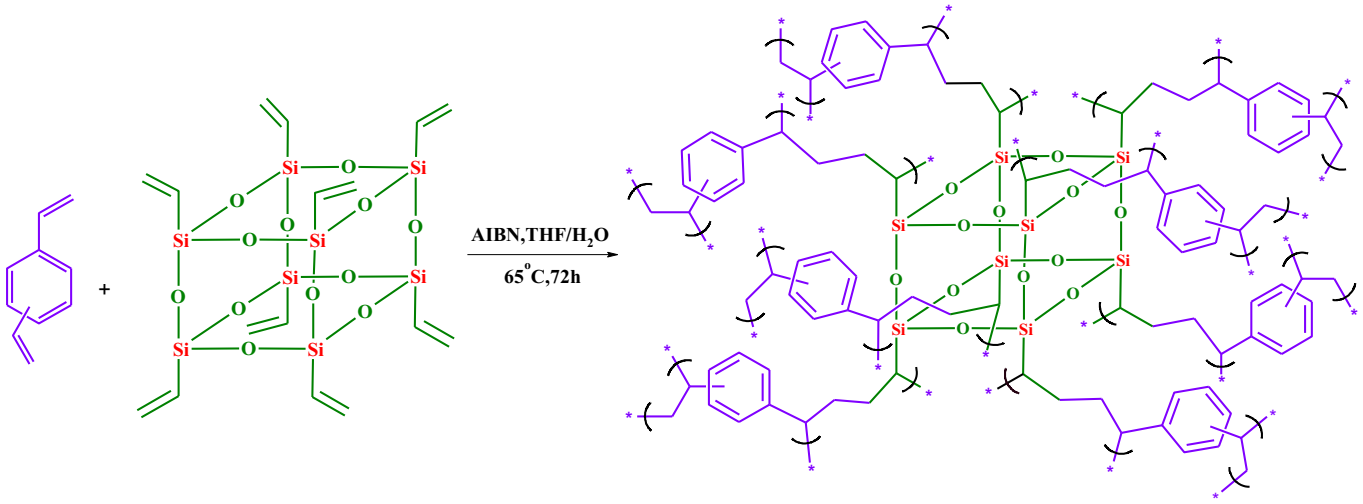

Fig. 1. Synthesis route of PDVB-POSS.

and b, ^{13}C and ^{1}H NMR spectra were measured to confirm the structure of octavinyl-POSS. In Fig. 2a, the chemical shift of CH═CH_2 present at 5.96 ppm and 6.06 ppm. The peak of the deuterated reagent appears at 7.26. Moreover, the resonance signal peaks appear at 128.8 ppm and 136.6 ppm in Fig. 2b were attributed to the signal peaks of CH═CH_2 [27]. The peak at 78 ppm was ascribed to deuterated reagent. Fig. 2c shows the results of the ^{13}C NMR solid spectra of PDVB and PDVB-POSS, they are very similar. For PDVB, the peaks at 128 ppm and

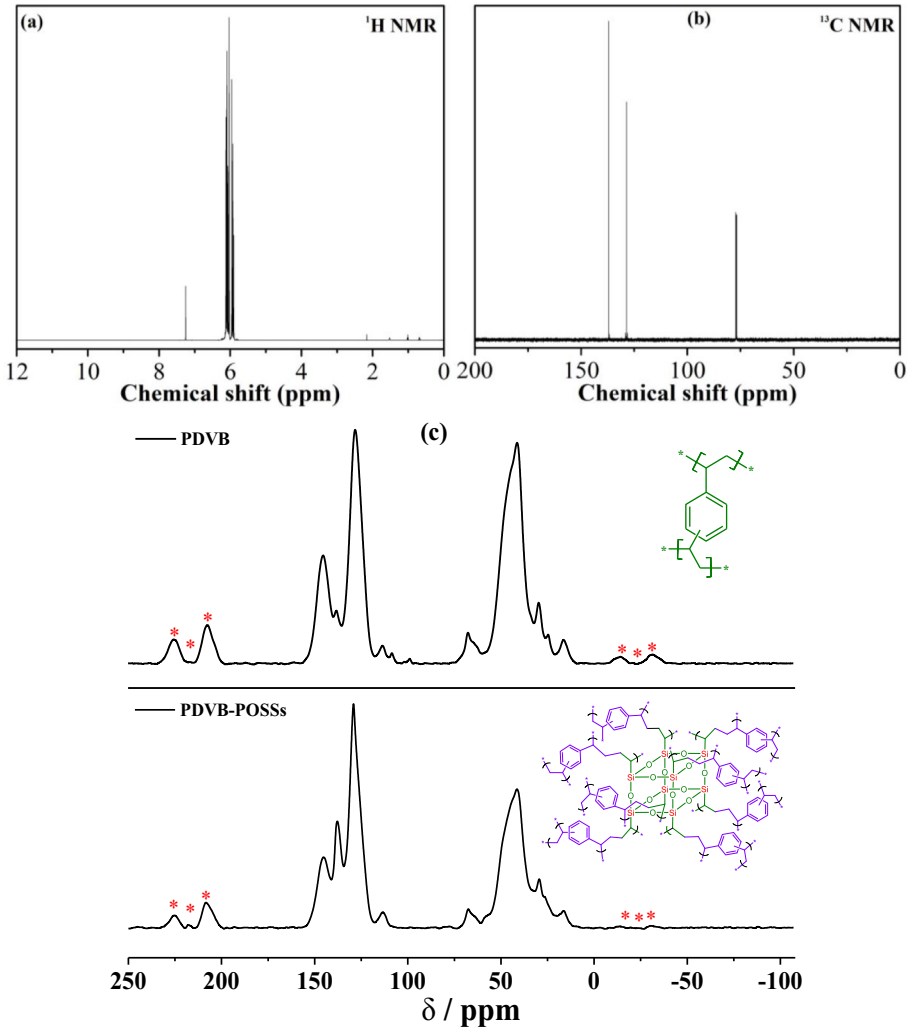

Fig. 2. (a) ^{1}H NMR spectra and (b) ^{13}C NMR spectra of octavinyl-POSS and (c) ^{13}C CP/MAS NMR spectra of PDVB and PDVB-POSS.

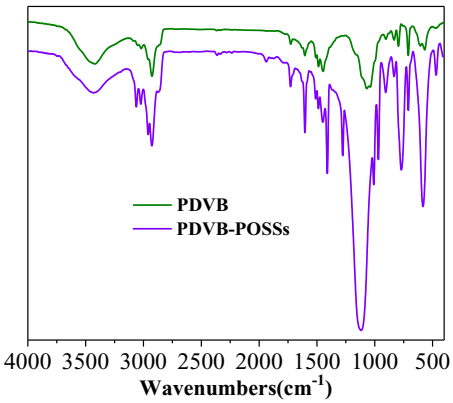

Fig. 3. FTIR spectra of PDVB and PDVB-POSS.

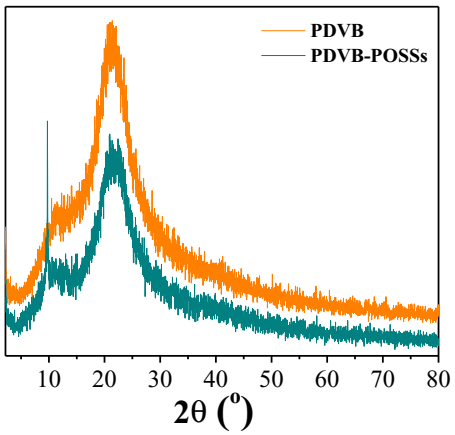

Fig. 5. XRD spectra of PDVB and PDVB-POSS.

138 ppm were attributed to the resonance of C_{Ar} site. The weak peak at 112 ppm was assigned to the terminal C═C. The peaks at 41 ppm was assigned to the resonance of −CH−CH_2− site [28], indicating that DVB has been polymerized. For PDVB-POSS, the peaks at 128 ppm, 138 ppm and 41 ppm were consistent with PDVB, indicating that DVB and octavinyl-POSS were successfully polymerized.

The structure of PDVB and PDVB-POSS were further analyzed by FTIR. The FTIR spectra of PDVB and PDVB-POSS as shown in Fig. 3, the main characteristic peaks of PDVB and PDVB-POSS are basically similar. A broad peak at 3400 cm^{-1} was ascribed to the O−H vibration, because of the presence of physically adsorbed water in the network structure. For PDVB, the characteristic absorption peaks in the range of 1450–1510 cm^{-1} were associated with the benzene ring skeleton stretching vibration. The characteristic peaks at 710 cm^{-1} and 795 cm^{-1} were attributed to the meta-substituted position on the benzene ring, and the peak at 833 cm^{-1} was ascribed to the para-substituted position on the benzene ring. In addition, the peak at 3020 cm^{-1} was classified as the stretching vibration of C_{AR}−H, and the range of 1000–1070 cm^{-1} were classified as the bending vibration of C_{AR}−H. The strong characteristic peak at 2926 cm^{-1} was ascribed to the stretching vibration of –CH2-, which indicates that DVB has been polymerized. As for PDVB-POSS, the peaks at 1410 cm^{-1} and 1276 cm^{-1} were attributed to the bending vibration of C−H. The peaks at 1118 cm^{-1} and 465 cm^{-1} were assigned to the stretching vibration of Si−O−Si, and the bending vibration of Si−O−Si at 583 cm^{-1}. The peak at 1603 cm^{-1} was assigned to the stretching vibration of the terminal C═C. After careful observation, it was found that the other absorption peak positions of PDVB-POSS were consistent with PDVB, indicating that the polymerization reaction occurred between DVB and octavinyl-POSS. Based on the analysis of FTIR and ^{13}C CP/MAS NMR, it was found that PDVB and PDVB-POSS were successfully synthesized

3.2. Morphological characterization

SEM was used to observe the micromorphology of PDVB and PDVB-POSS, as shown in Fig. 4. It can be clearly seen that the morphology of

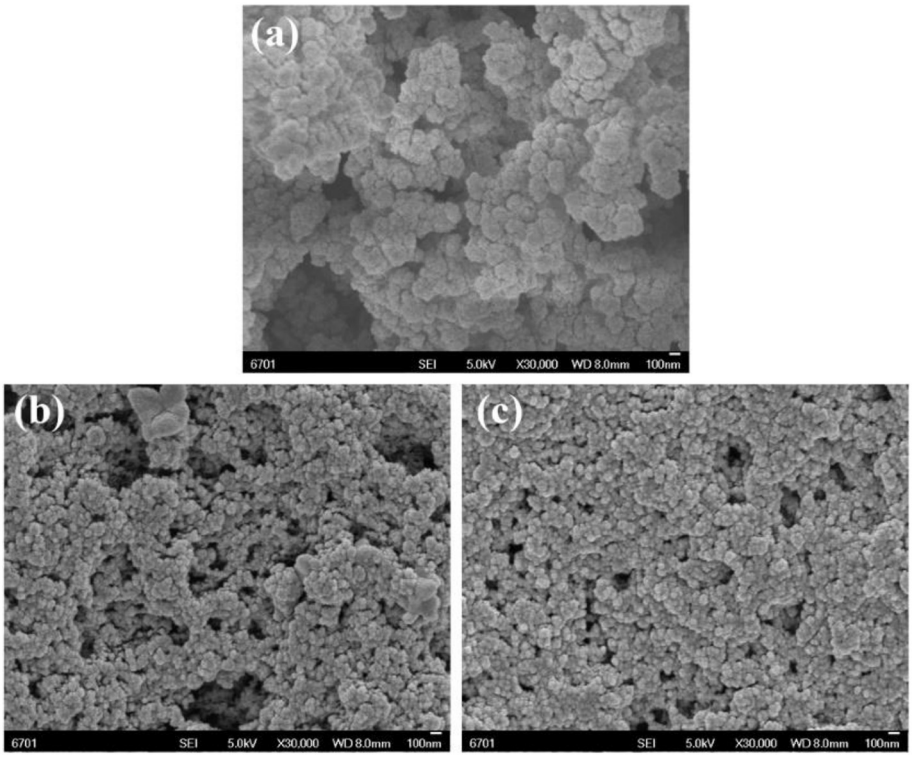

Fig. 4. SEM images of PDVB (a) and PDVB-POSS (b, c). Scale bar: (a,b,c) 100 nm.

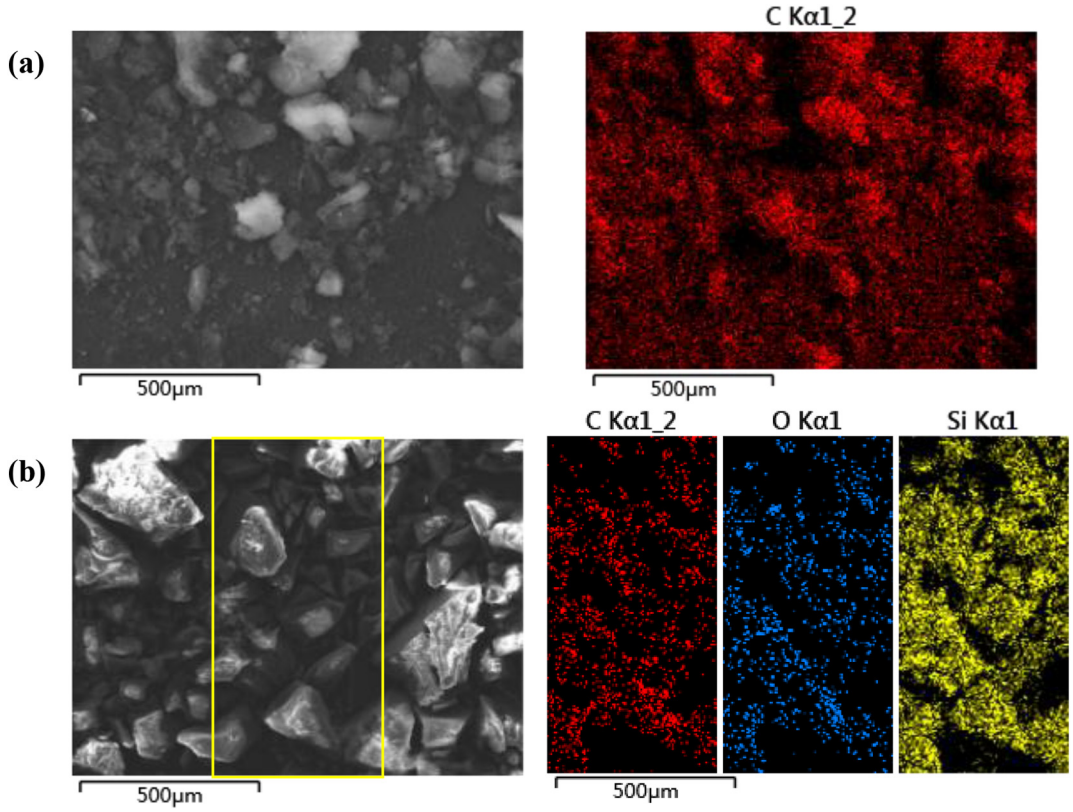

Fig. 6. (a) SEM image of PDVB and EDX carbon mapping of the region shown in (a), (b) SEM image of PDVB-POSS and EDX carbon, oxygen and silicon mapping of the region shown in (b). Scale bar: (a,b) 500 μm.

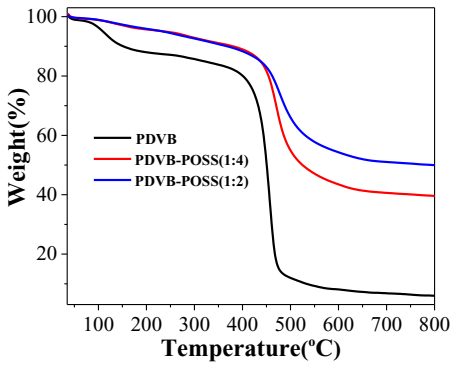

Fig. 7. TGA curves of PDVB and PDVB-POSS under nitrogen.

PDVB and PDVB-POSS are different. The PDVB exhibits a large deposit of small particles (Fig. 4a), and possesses a porous three dimensional network structure with a heterogeneous pore size distribution, mainly composed of mesopores and macropores. The PDVB-POSS (1:4) is also composed of a large number of small particles, which is accompanied by partial agglomeration (Fig. 4b). The porous structure of PDVB-POSS (1:4) is also dominated by mesopores and macropores. The PDVB-POSS (1:2) is composed of relatively uniform irregular spherical particles (Fig. 4c), which are arranged very tightly to make the pore size significantly smaller than PDVB and PDVB-POSS (1:4). Obviously, as the monomer content increases, the pore size of PDVB-POSS is decreases and the particle agglomeration of PDVB-POSS is increases, which indicates that the molar ratio of octavinyl-POSS and DVB has a greater influence on the morphology of PDVB-POSS. The difference in morphology has stimulated our interest in exploring crystal forms of PDVB and PDVB-POSS. The XRD spectra of PDVB and PDVB-POSS were performed to analyze their crystal forms. Fig. 5 shows both PDVB and PDVB-POSS have a large broad peak at about 22°, which was associated with the diffraction pattern of a typical amorphous polymer. For PDVB-POSS, the peak present about 9° is ascribed the POSS [29], which confirm the presence of POSS moieties in the polymer.

3.3. Surface chemical characterization

To determine the distribution of individual elements in PDVB and PDVB-POSS, the elemental mapping of PDVB and PDVB-POSS were further observed by scanning electron microscopy with energy dispersive X-ray (SEM-EDX) [30], the results as shown in Fig. 6. The PDVB is mainly composed of C element, Fig. 6a shows SEM image and C mapping of the region of the PDVB. Apparently, the main element in PDVB is the C element, which is consisted with the composition of C element in the PDVB skeleton. Similarly, the PDVB-POSS is mainly composed of C element, Si element and O element, Fig. 6b shows SEM image and the C mapping, Si mapping and O mapping of the region of the PDVB-POSS. Obviously, the C elements, Si element and O element were uniformly distributed in the skeleton of PDVB-POSS, it was beneficial for the flame retardant experiment. The SEM-EDX results further confirm that PDVB and PDVB-POSS are successfully synthesized by solvothermal methods.

3.4. Thermal stability

TGA was used to characterize the thermal stability of PDVB and two PDVB-POSS. For PDVB and PDVB-POSS, the TGA tests are performed in nitrogen atmosphere and the results are shown in Fig. 7. The mass loss of PDVB is 12% in the temperature range from room temperature to 200 °C due to the breakage of the oligomer in PDVB. The thermal decomposition temperature of PDVB is about 450 °C. When the temperature reaches 800 °C, the mass loss of PDVB reached nearly 92%. It can be clearly observed that the thermal stability of PDVB-POSS is

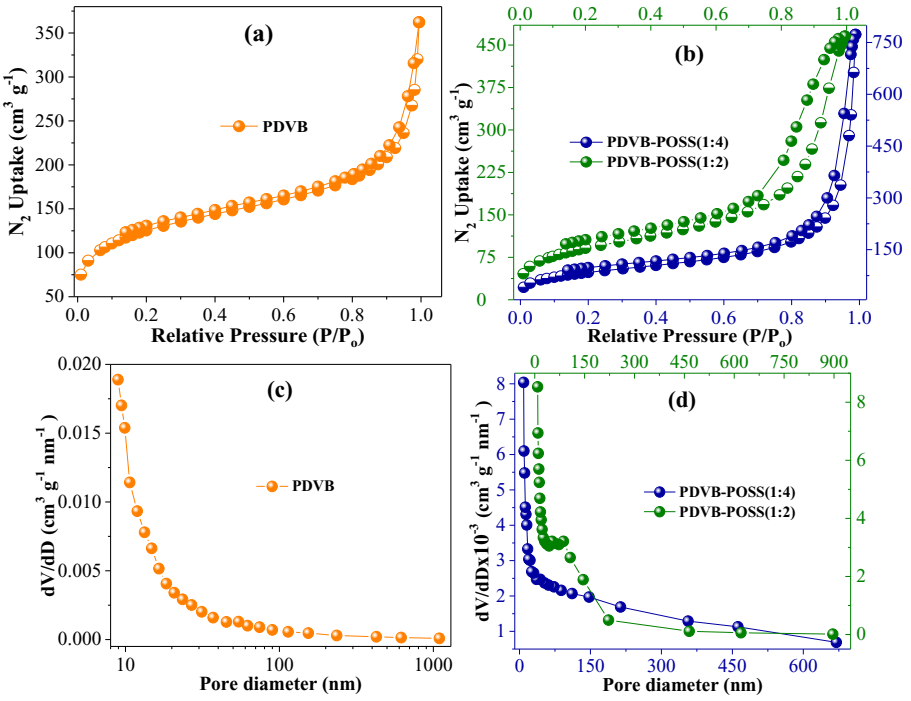

Fig. 8. Nitrogen adsorption and desorption isotherms of PDVB measured at 77.3 K, (b) Nitrogen adsorption and desorption isotherms of PDVB-POSS(1:4) and PDVB-POSS(1:2) measured at 77.3 K, (c) Pore size distribution for PDVB, calculated according to desorption data, (d) Pore size distribution for PDVB-POSS (1:4) and PDVB-POSS(1:2) calculated according to desorption data (filled circles: adsorption, semi-filled circles: desorption).

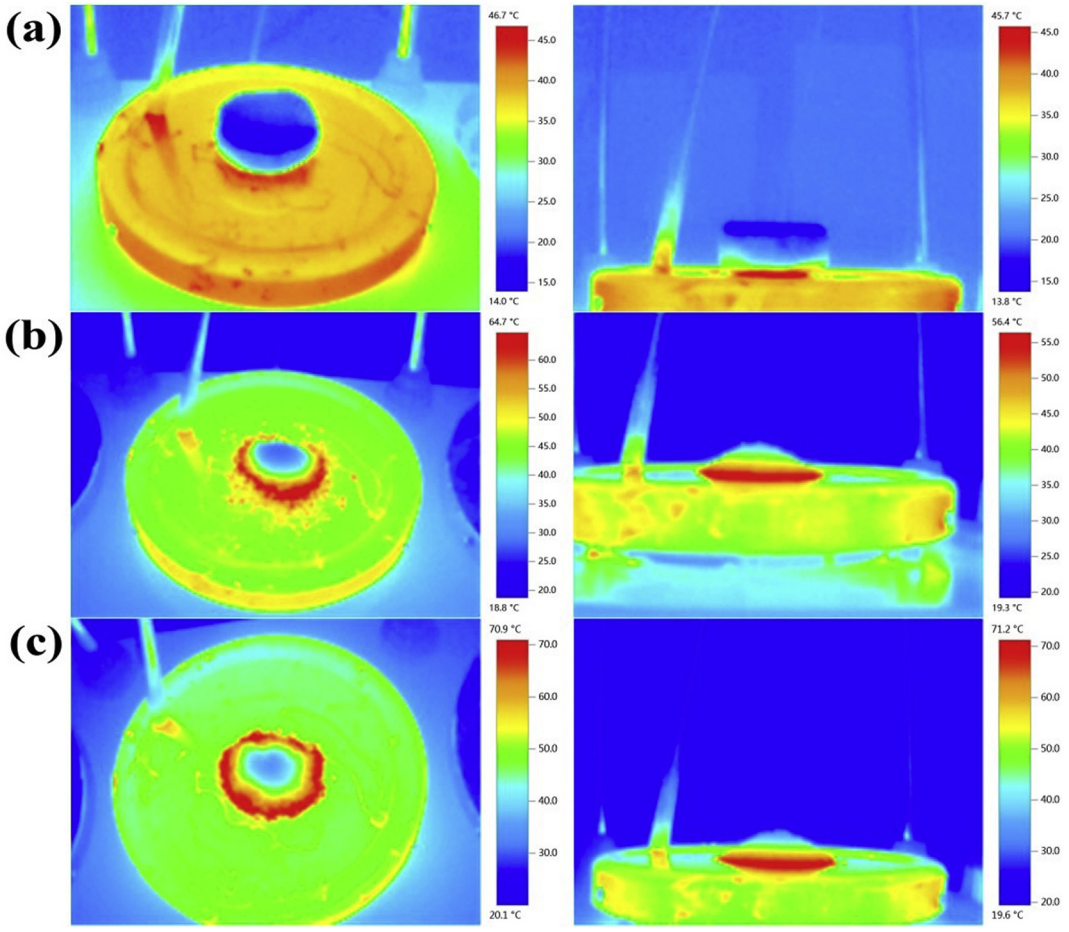

Fig. 9. Thermographic images of (a) PDVB, (b) PDVB-POSS(1:4) and (c) PDVB-POSS(1:2).

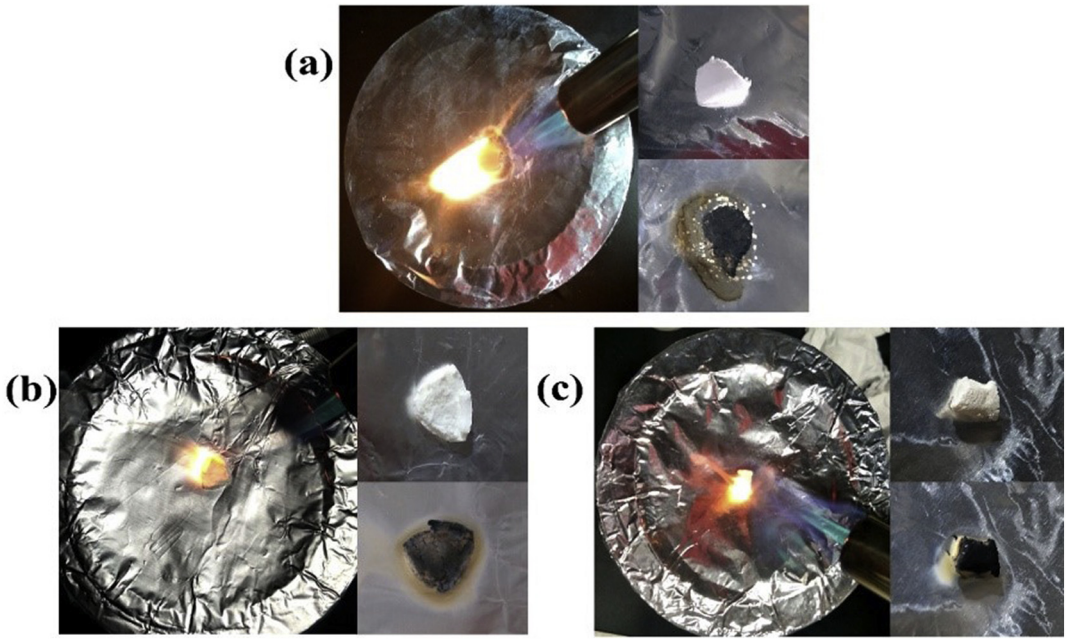

Fig. 10. Digital photos of (a) PDVB, (b) PDVB-POSS(1:4) and (c) PDVB-POSS(1:2) burning tests and before (above) and after (under) the tests.

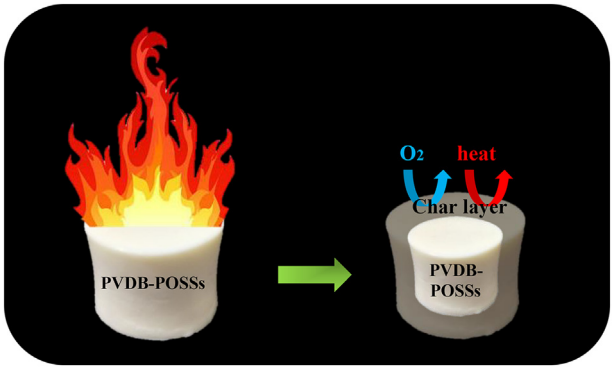

Fig. 11. Schematic illustration of the flame retardant mechanism of PDVB-POSS.

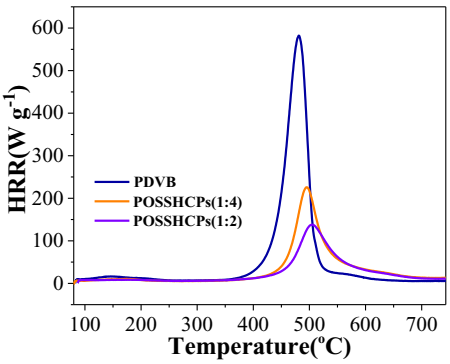

Fig. 12. HRR curves of PDVB and PDVB-POSS.

significantly superior to PDVB. The mass loss of PDVB-POSS was less than that of PDVB before 200 °C, indicating that a bit of oligomers was formed in PDVB-POSS. The mass loss of PDVB-POSS in only 15% as the temperature up to 450 °C, and the thermal decomposition temperature of PDVB-POSS was about 480 °C. At 800 °C, the mass loss of PDVB-POSS (1:4) and PDVB-POSS (1:2) is 60% and 47%, respectively. The analysis of TGA shows that PDVB-POSS have outstanding thermal stability. It also shows that the thermal stability and decomposition temperature of PDVB-POSS are in direct proportion to the content of octavinyl-POSS.

3.5. Porosity properties

BET was used to analyze the porosity properties of PDVB and PDVB-POSS by the N_2 adsorption and desorption tests at 77.3 K, as shown in Fig. 8. According to the classification of IUPAC, PDVB and PDVB-POSS give rise to type-II/IV mixed nitrogen adsorption isotherms [31–33]. PDVB and PDVB-POSS exhibit strong nitrogen adsorption (shown in Fig. 8a and b) at a relative pressure (P/P_0) range from 0.8 to 1.0, demonstrating the presence of macropores in PDVB and PDVB-POSS. Furthermore, hysteresis loops exist in PDVB and PDVB-POSS due to the elastic deformation or swelling effect caused by the adsorption gas of the polymer [34]. The pore performance data of PDVB and PDVB-POSS are presented in Table S1. The apparent BET surface areas of PDVB, PDVB-POSS (1:4) and PDVB-POSS (1:2) were 417 $m^2 g^{-1}$, 298 $m^2 g^{-1}$ and 319 $m^2 g^{-1}$, respectively. The micropores surface area of PDVB was calculated to be 97 $m^2 g^{-1}$ using t-plot method, while the micropores surface areas of PDVB-POSS (1:4) and PDVB-POSS (1:2) were 4 $m^2 g^{-1}$ and 8 $m^2 g^{-1}$, respectively. And the total pore volume are 0.495 $cm^3 g^{-1}$ for PDVB, 1.026 $cm^3 g^{-1}$ for PDVB-POSS(1:4) and 0.705 $cm^3 g^{-1}$ for PDVB-POSS(1:2). Besides, the pore size distribution (PSD) curves (shown in Fig. 8c and Fig. 8d) of PDVB and PDVB-POSS show that the polymer mainly contain microporous and mesoporous, and the adsorption average pore width was calculated to be 4.7 nm, 13.8 nm and 8.8 nm for PDVB, PDVB-POSS (1:4) and PDVB-POSS (1:2), respectively.

3.6. Thermal insulation and combustion properties

To investigate the thermal insulation properties of PDVB and PDVB-POSS, the thermal conductivity of the three polymers were measured under ambient temperature and pressure, and the results are shown in Table S2. The thermal conductivity of PDVB, PDVB-POSS (1:4) and PDVB-POSS (1:2) was 0.018 $W m^{-1} k^{-1}$, 0.024 $W m^{-1} k^{-1}$ and 0.032 $W m^{-1} k$, respectively. The thermal conductivity values of the three polymers are lower than traditional thermal insulation materials [35–37], thus they can be used as thermal insulation materials. For PDVB, it has a large number of microporous structures, which can

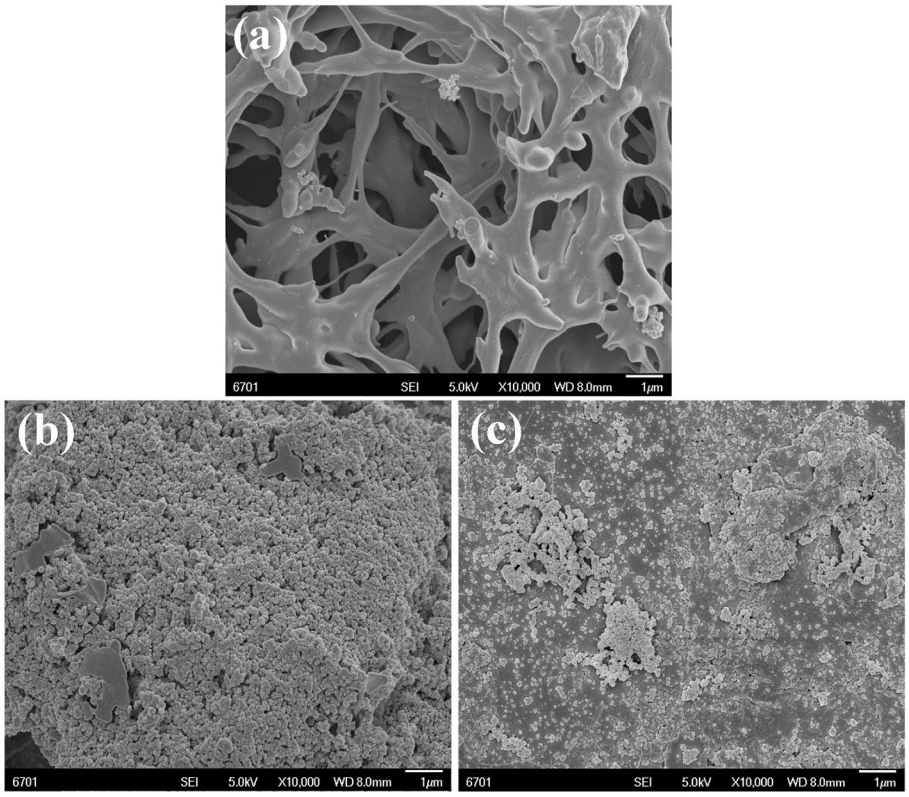

Fig. 13. SEM images of (a) PDVB-C1, (b) PDVB-POSS(1:4)-C2 and (c) PDVB-POSS(1:2)-C2. Scale bar: (a, b, c) 1 μm.

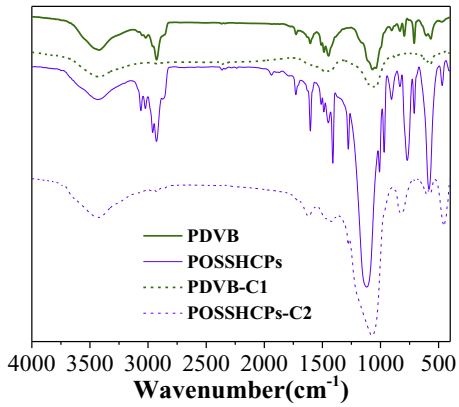

Fig. 14. FT-IR spectra of PDVB and PDVB-POSS and the same polymer after burning tests.

restrict the relative motion of air molecules to reduce thermal convection, thereby giving the polymer a lower thermal conductivity. PDVB-POSS also have some microporous structures, but the number of microporous is much less than that of PDVB. Therefore, the thermal conductivity of PDVB-POSS is higher than that of PDVB. What's more, the thermal conductivity of PDVB-POSS is increased with the increase of POSS content, which makes the polymer denser lead to the thermal insulation properties of the polymer was weakened.

To observe the thermal insulation performance of PDVB and PDVB-POSS, we further verified with thermographic images, as shown in Fig. 9. The temperature distribution of PDVB and PDVB-POSS can be clearly observed by the colors of the thermographic images. The PDVB (thickness is 1.3 cm) was placed on the heating plate to form a larger temperature gradient ($dT/dx = 21.5\ ^{\circ}C\ cm^{-1}$), indicating that PDVB can effectively prevent the transmission of heat, so PDVB has excellent thermal insulation properties. On the contrary, the thermal insulation of PDVB-POSS is relatively weak, and the temperature gradient of PDVB-POSS (1:4) and PDVB-POSS (1:2) are $19.1\ ^{\circ}C\ cm^{-1}$ and $17.9\ ^{\circ}C\ cm^{-1}$, respectively. From the values of temperature gradient, it was found that the thermal insulation properties of PDVB and PDVB-POSS are consistent with the results of thermal conductivity.

The combustion performance of PDVB and PDVB-POSS were initially studied by torch combustion tests. PDVB and PDVB-POSS were directly exposed to the blue flame of butane, which was remained stationary and maintained at a 45° angle with the horizontal direction, and the combustion results are shown in Fig. 10. When PDVB is exposed to a butane flame, it ignites immediately and the bright flame spreads rapidly around. After the test, the sample burned more thoroughly and the surface of the residue was cracked. PDVB-POSS also ignited when exposed to a butane flame, but the flame spreads slowly and not bright enough. At the same time, the residue of PDVB-POSS basically retained original shape without collapsing. And a tight and complete char layer was observed for PDVB-POSS (1:2), it acts as a barrier to block heat and oxygen from diffusing to the substrate material. In addition, POSS contains a large amount of Si element, which formed SiO_2 after pyrolysis to contribute the formation of char layer. Therefore, with increasing Si content, the flame retardancy of PDVB-POSS elevated. These phenomena indicate that the introduction of octavinyl-POSS into the polymer should be able to improve its flame retardancy. And the flame retardant mechanism is shown in Fig. 11.

MCC was used to obtain the information on the combustion properties of PDVB and PDVB-POSS to further investigate the flammability of PDVB and PDVB-POSS, including the heat release rate (HRR), peak heat release rate (pHRR), heat release capacity (HR capacity), total heat release (THR) and the temperature (T_{max}) corresponding to the peak heat release rate. All the test data are shown in Fig. 12 and Table S3. For HRR cures, we observed that the HRR value of PDVB increased rapidly and reached $576\ W\ g^{-1}$, implying that PDVB burning quickly after ignition. For PDVB-POSS(1:4) and PDVB-POSS(1:2), the pHRR are $218.2\ W\ g^{-1}$ (reduce at least 62.1%) and $129.3\ W\ g^{-1}$ (reduce at least

77.6%), respectively. Therefore, PDVB-POSS could be effectively reduced the risk of fire. What is more, the HR capacity and THR of PDVB-POSS are clearly lower than PDVB. These indicating that the introduction of octavinyl-POSS in the polymer can significantly improve its flame retardancy. And with the increase of octavinyl-POSS content, the flame retardancy of the polymer is enhanced. The MCC results show that PDVB-POSS have outstanding flame retardancy.

The morphology of PDVB-C1, PDVB-POSS (1:4)-C2 and PDVB-POSS (1:2)-C2 was observed by SEM, and the results are shown in Fig. 13. Obviously, PDVB-C1 and PDVB-POSS-C2 have different appearances. The PDVB-C1 exhibits a three-dimensional network structures with a large number of macroporous and the skeleton was fractured, proves that the material is fully burned. Contrarily, PDVB-POSS (1:4)-C2 is composed by the accumulation of nanoparticles with a rough surface, and the diameter of the pore is significantly reduced. Compared with PDVB-POSS (1:4)-C2, the surface of PDVB-POSS(1:2)-C2 is smoother and more regular, without cracks. These char layer would effectively protect the substrate material form further burning.

The structures of the residual chars (named as PDVB-C1 and PDVB-POSS-C2, respectively.) for PDVB and PDVB-POSS were analyzed by FT-IR. The FT-IR spectra of PDVB and PDVB-POSS before and after combustion as shown in Fig. 14. Compared with PDVB and PDVB-POSS, the FTIR spectra of PDVB-C1 and PDVB-POSS-C2 have significant changed. After combustion, the characteristic peaks in the range of 3200–2900 cm^{-1} disappeared, and the characteristic peaks of the meta-substituted position (710 cm^{-1} and 795 cm^{-1}) and para-substituted position (833 cm^{-1}) on the benzene ring were also disappeared, indicating that the structure of PDVB and PDVB-POSS has substituted. For PDVB-POSS-C2, the peaks at 465 cm^{-1} and 583 cm^{-1} were attributed to the stretching and bending vibration of Si—O—Si, indicating that an antioxidant protective layer is formed in the residue of PDVB-POSS to enhance its flame retardancy.

4. Conclusions

In summary, we have demonstrated a simple method for engineering of POSS-based polymers into monolithic scaffold with porous feature as efficient flame retardant with good thermal insulation. The as-prepared PDVB-POSS show high thermal insulation with a low thermal conductivity of 0.024 $W\,m^{-1}\,k^{-1}$ in air. Taking advantages of the rigid structure of PDVB-POSS, the PDVB-POSS possesses excellent flame retardancy with a peak heat released rate of as low as 144 $W\,g^{-1}$ as well as self-extinguishing behaviors without generation of any melt dripping. In such testing, the formation of condensed carbon layer coupled with and three-dimensional nanoporous structure could act as heat barrier to impede and retard the oxygen, mass and heat transfer to substrate when it undergoes high temperature treatment. Taking advantages of simple fabrication process, easily to be scaled-up, excellent thermal insulation and flame retardancy, such POSS-based monolithic porous polymers may have great potential as energy-saving coatings for real applications.

Author contributions

An Li has a holistic grasp of the central thought of the whole article; Fei Wang, Huijuan Wei, Wanli Zhang, Chao Liu, Hanxue Sun, Zhaoqi Zhu, Weidong Liang, An Li * provided technical support. All authors co-wrote the manuscript.

Declaration of Competing Interest

There are no conflicts to declare.

Acknowledgment

The authors are grateful to the National Natural Science Foundation of China (Grant No. 51663012, 21975113, 51962018), the Natural Science Foundation of Gansu Province, China (Grant No. 1610RJYA001), Support Program for Hongliu Young Teachers (Q201411), Hongliu Elitist Scholars of LUT (J201401), Support Program for Longyuan Youth and Fundamental Research Funds for the Universities of Gansu Province, Project of Collaborative Innovation Team, Innovation and Entrepreneurship Talent Project of Lanzhou (2017-RC-33).

Appendix A. Supplementary data

Supplementary data to this article can be found online at https://doi.org/10.1016/j.reactfunctpolym.2019.104345.

References

[1] P.H. Shaikh, N.B.M. Nor, P. Nallagownden, I. Elamvazuthi, T. Ibrahim, Renew. A review on optimized control systems for building energy and comfort management of smart sustainable buildings, Renew. Sust. Energ. Rev. 34 (2014) 409–429.
[2] D. Ürge-Vorsatz, L.F. Cabeza, S. Serrano, C. Barreneche, K. Petrichenko, Renew. Heating and cooling energy trends and drivers in buildings, Renew. Sust. Energ. Rev. 41 (2015) 85–98.
[3] G. Laufer, C. Kirkland, A.A. Cain, J.C. Grunlan, Clay–chitosan nanobrick walls: completely renewable gas barrier and flame-retardant nanocoatings, ACS Appl. Mater. Interfaces 4 (3) (2012) 1643–1649.
[4] O. Köklükaya, F. Carosio, J.C. Grunlan, L. Wagberg, Flame-retardant paper from wood fibers functionalized via layer-by-layer assembly, ACS Appl. Mater. Interfaces 7 (42) (2015) 23750–23759.
[5] Medved S.; Lesar B.; Tudor E., Thermal insulation panels from cellulosic fibres, Forest Prod. J., 2015, 65(3–4): S54-S54. Academic OneFile,.
[6] A. Briga-Sá, D. Nascimento, N. Teixeira, J. Pinto, F. Caldeira, H. Varum, A. Paiva, Textile waste as an alternative thermal insulation building material solution, Constr. Build. Mater. 38 (2013) 155–160.
[7] A. Kumar, B.M. Suman, Experimental evaluation of insulation materials for walls and roofs and their impact on indoor thermal comfort under composite climate, Build. Environ. 59 (2013) 635–643.
[8] O. Kaynakli, A review of the economical and optimum thermal insulation thickness for building applications, Renew. Sust. Energ. Rev. 16 (1) (2012) 415–425.
[9] Z. Zhang, P. Mu, J. He, Z. Zhu, H. Sun, H. Wei, W. Liang, A. Li, Facile and scalable fabrication of surface-modified sponge for efficient solar steam generation, Chem. Sus. Chem. 12 (2) (2019) 426–433.
[10] F. Wang, D. Wei, Y. Li, T. Chen, P. Mu, H. Sun, Z. Zhu, W. Liang, A. Li, Chitosan/reduced Graphene oxide modified spacer fabric as salt-resistant solar absorber for efficient solar steam generation, J. Mater. Chem. A 7 (31) (2019) 18311–18317.
[11] G. Hayase, K. Kanamori, K. Abe, H. Yano, A. Maeno, H. Kaji, K. Nakanishi, Polymethylsilsesquioxane–cellulose nanofiber biocomposite aerogels with high thermal insulation, bendability, and superhydrophobicity, ACS Appl. Mater. Interfaces 6 (12) (2014) 9466–9471.
[12] L. Yang, A. Mukhopadhyay, Y. Jiao, Q. Yong, L. Chen, Y. Xing, J. Hamel, H. Zhu, Ultralight, highly thermally insulating and fire resistant aerogel by encapsulating cellulose nanofibers with two-dimensional MoS_2, Nanoscale 9 (32) (2017) 11452–11462.
[13] N. Sarier, E. Onder, Thermal insulation capability of PEG-containing polyurethane foams, Thermochim. Acta 475 (1–2) (2008) 15–21.
[14] G. Hayase, K. Nonomura, K. Kanamori, A. Maeno, H. Kaji, K. Nakanishi, Boehmite nanofiber–polymethylsilsesquioxane core–shell porous monoliths for a thermal insulator under low vacuum conditions, Chem. Mater. 28 (10) (2016) 3237–3240.
[15] L. Huan, X. Shen, W. Xinwei, M. Ning, Significantly reduced thermal diffusivity of free-standing two-layer graphene in graphene foam, Nanotechnology 24 (41) (2013) 415706.
[16] Y. Wang, X. Yang, P. Hui, W. Fang, L. Xiu, Y. Yang, J. Hao, Layer-by-layer assembly of multifunctional flame retardant based on brucite, 3-aminopropyltriethoxysilane, and alginate and its applications in ethylene-vinyl acetate resin, ACS Appl. Mater. Interfaces 8 (15) (2016) 9925–9935.
[17] H. Pan, W. Wang, Y. Pan, L. Song, Y. Hu, K.M. Liew, Formation of layer-by-layer assembled titanate nanotubes filled coating on flexible polyurethane foam with improved flame retardant and smoke suppression properties, ACS Appl. Mater. Interfaces 7 (1) (2014) 101–111.
[18] O. Köklükaya, F. Carosio, J.C. Grunlan, L. Wagberg, Flame-retardant paper from wood fibers functionalized via layer-by-layer assembly, ACS Appl. Mater. Interfaces 7 (42) (2015) 23750–23759.
[19] Y. Wang, Z. Li, Y. Li, J. Wang, X. Liu, T. Song, X. Yang, J. Hao, Spray-drying-assisted layer-by-layer assembly of alginate, 3-Aminopropyltriethoxysilane, and magnesium hydroxide flame retardant and its catalytic graphitization in ethylene–vinyl acetate resin, ACS Appl. Mater. Interfaces 10 (12) (2018) 10490–10500.
[20] H. Wei, F. Wang, H. Sun, Z. Zhu, C. Xiao, W. Liang, B. Yang, L. Chen, A. Li, Benzotriazole-based conjugated microporous polymers as efficient flame retardants with better thermal insulation properties, J. Mater. Chem. A 6 (18) (2018) 8633–8642.
[21] H. Wei, F. Wang, X. Qian, S. Li, Z. Hu, H. Sun, Z. Zhu, W. Liang, C. Ma, A. Li, Superhydrophobic fluorine-rich conjugated microporous polymers monolithic

nanofoam with excellent heat insulation property, Chem. Eng. J. 351 (2018) 856–866.
[22] C. Zhang, F. Babonneau, C. Bonhomme, R.M. Laine, C.L. Soles, H.A. Hristov, A.F. Yee, Highly porous polyhedral silsesquioxane polymers. Synthesis and characterization, J. Am. Chem. Soc. 120 (33) (1998) 8380–8391.
[23] M. Ge, H. Liu, A silsesquioxane-based thiophene-bridged hybrid nanoporous network as a highly efficient adsorbent for wastewater treatment, J. Mater. Chem. A 4 (42) (2016) 16714–16722.
[24] H. Liu, H. Liu, Selective dye adsorption and metal ion detection using multifunctional silsesquioxane-based tetraphenylethene-linked nanoporous polymers, J. Mater. Chem. A 5 (19) (2017) 9156–9162.
[25] X. Yang, H. Liu, Ferrocene-functionalized silsesquioxane-based porous polymer for efficient removal of dyes and heavy metal ions, Chem. Eur. J. 24 (51) (2018) 13504–13511.
[26] Y. Du, M. Ge, H. Liu, Porous polymers derived from octavinylsilsesquioxane by cationic polymerization, Macromol. Chem. Phys. 220 (5) (2019) 1800536.
[27] D. Chen, S. Yi, W. Wu, Y. Zhong, J. Liao, C. Huang, W. Shi, Synthesis and characterization of novel room temperature vulcanized (RTV) silicone rubbers using vinyl-POSS derivatives as cross linking agents, Polymer 51 (17) (2010) 3867–3878.
[28] F. Liu, X. Meng, Y. Zhang, L. Ren, F. Nawaz, F.-S. Xiao, Efficient and stable solid acid catalysts synthesized from sulfonation of swelling mesoporous polydivinylbenzenes, J. Catal. 271 (1) (2010) 52–58.
[29] A.J. Waddon, E.B. Coughlin, Crystal structure of polyhedral oligomeric silsequioxane (POSS) nano-materials: a study by X-ray diffraction and electron microscopy, Chem. Mater. 15 (24) (2003) 4555–4561.
[30] P. Mu, W. Bai, Y. Fan, Z. Zhang, H. Sun, Z. Zhu, W. Liang, A. Li, Conductive hollow kapok fiber-PPy monolithic aerogels with excellent mechanical robustness for efficient solar steam generation, J. Mater. Chem. A 7 (16) (2019) 9673–9679.
[31] M. Thommes, K. Kaneko, A.V. Neimark, J.P. Olivier, F. Rodriguezreinoso, J. Rouquerol, K.S.W. Sing, Physisorption of gases, with special reference to the evaluation of surface area and pore size distribution (IUPAC technical report), Pure Appl. Chem. 87 (9–10) (2015) 1051–1069.
[32] P. Mu, Z. Zhang, W. Bai, J. He, H. Sun, Z. Zhu, W. Liang, A. Li, Superwetting monolithic hollow-carbon-nanotubes aerogels with hierarchically nanoporous structure for efficient solar steam generation, Adv. Energy Mater. 9 (1) (2019) 1802158.
[33] P. Mu, W. Bai, Z. Zhang, J. He, H. Sun, Z. Zhu, W. Liang, A. Li, Robust aerogels based on conjugated microporous polymer nanotubes with exceptional mechanical strength for efficient solar steam generation, J. Mater. Chem. A 6 (37) (2018) 18183–18190.
[34] J. He, G. Zhao, P. Mu, Y. Su, H. Sun, Z. Zhu, W. Liang, A. Li, Scalable fabrication of monolithic porous foam based on cross-linked aromatic polymers for efficient solar steam generation, Sol. Energ. Mat. Sol. C. 201 (2019) 110111.
[35] H. Binici, M. Eken, M. Dolaz, O. Aksogan, M. Kara, An environmentally friendly thermal insulation material from sunflower stalk, textile waste and stubble fibres, Constr. Build. Mater. 51 (2014) 24–33.
[36] G. Xue, K. Liu, Q. Chen, P. Yang, J. Li, T. Ding, J. Duan, B. Qi, J. Zhou, Robust and low-cost flame-treated wood for high-performance solar steam generation, ACS Appl. Mater. Interfaces 9 (17) (2017) 15052–15057.
[37] B.P. Jelle, Traditional, state-of-the-art and future thermal building insulation materials and solutions–properties, requirements and possibilities, Energ. Buildings 43 (10) (2011) 2549–2563.